Global Precipitation: A 17-Year Monthly Analysis Based on Gauge Observations, Satellite Estimates, and Numerical Model Outputs

Pingping Xie and Phillip A. Arkin
National Centers for Environmental Prediction,
National Oceanic and Atmospheric Administration, Washington, D.C.

ABSTRACT

Gridded fields (analyses) of global monthly precipitation have been constructed on a 2.5° latitude–longitude grid for the 17-yr period from 1979 to 1995 by merging several kinds of information sources with different characteristics, including gauge observations, estimates inferred from a variety of satellite observations, and the NCEP–NCAR reanalysis. This new dataset, which the authors have named the CPC Merged Analysis of Precipitation (CMAP), contains precipitation distributions with full global coverage and improved quality compared to the individual data sources. Examinations showed no discontinuity during the 17-yr period, despite the different data sources used for the different subperiods. Comparisons of the CMAP with the merged analysis of Huffman et al. revealed remarkable agreements over the global land areas and over tropical and subtropical oceanic areas, with differences observed over extratropical oceanic areas. The 17-yr CMAP dataset is used to investigate the annual and interannual variability in large-scale precipitation. The mean distribution and the annual cycle in the 17-yr dataset exhibit reasonable agreement with existing long-term means except over the eastern tropical Pacific. The interannual variability associated with the El Niño–Southern Oscillation phenomenon resembles that found in previous studies, but with substantial additional details, particularly over the oceans. With complete global coverage, extended period and improved quality, the 17-yr dataset of the CMAP provides very useful information for climate analysis, numerical model validation, hydrological research, and many other applications. Further work is under way to improve the quality, extend the temporal coverage, and to refine the resolution of the merged analysis.

1. Introduction

Despite the increasing requirements for high-quality precipitation datasets from both the meteorological and hydrological communities, accurate quantitative documentation of global precipitation remains as one of the major challenges for scientists working on technique development and dataset construction, principally because of the large spatial and temporal variability in precipitation and because of the lack of a comprehensive observing system (WCRP 1993). The major existing sources of large-scale precipitation data include gauge observations, estimates inferred from satellite observations, and outputs from various numerical models, each of which has advantages as well as shortcomings.

Generally speaking, rain gauges give relatively accurate point measurements of precipitation but suffer from sampling error in representing area means and are not available over most oceanic and unpopulated land areas. Satellite observations of infrared (IR) and microwave (MW) radiance have been used successfully to retrieve precipitation information over many parts of the globe (Barrett and Martin 1981; Arkin and Ardanuy 1989), but the estimates made from satellite observations contain nonnegligible random error and bias because of the indirect nature of the relationship between the observation and the precipitation, the inadequate sampling, and algorithm imperfections. In general, different satellite estimates based on a given sort of observation data (IR, MW scattering, or MW emission) exhibit similar skills, while those based on

Corresponding author address: Dr. Pingping Xie, National Centers for Environmental Prediction, #800A, NOAA/NWS, Washington, DC 20233.
E-mail: xping@sgi17.wwb.noaa.gov
In final form 25 June 1997.

different sources of data vary more from one another in their performance in estimating precipitation over various areas and for various seasons. In general, however, most such estimates yield relatively good (poor) results for tropical oceanic (cold season extratropical land) precipitation (Xie and Arkin 1995; Janowiak et al. 1995). The precipitation distributions produced by various numerical models, meanwhile, exhibit relatively high quality in mid- and high latitudes but perform more poorly over most tropical areas (Arpe 1991). After a comprehensive examination of several individual datasets of large-scale precipitation, Xie and Arkin (1995) concluded that all of these individual data sources present similar distribution patterns of large-scale precipitation but with differences in smaller-scale features and in amplitudes and that at least three major deficiencies exist in the individual data sources: 1) incomplete global coverage, 2) significant random error, and 3) nonnegligible bias.

Acknowledgment of the limitations inherent in the individual sources of large-scale precipitation has led to some recent attempts to combine them so as to take advantage of the strengths of each to produce the best possible analysis (gridded field) of global precipitation. One such effort is reported by Adler et al. (1993, 1994), Huffman et al. (1995), and Huffman et al. (1997). Assuming that estimates based on MW observations from the Special Sensor Microwave/Imager (SSM/I) on board the DMSP satellites give relatively accurate instantaneous rain rate but with poor sampling in time and that the GOES Precipitation Index (GPI; Arkin and Meisner 1987) estimates based on IR observations from geostationary satellites provide frequent coverage but with significant bias, Adler et al. (1993) and Adler et al. (1994) calculate the ratio between the MW and the GPI estimates when both are available and use the ratio to adjust the GPI estimates. Their multisatellite (MS) estimates, comprised of the adjusted GPI from 40°S to 40°N and the MW estimates elsewhere, are then multiplied by the ratio between the concurrent gauge observations and the MS calculated over a large-scale area to correct the bias. Finally, gauge observations are combined with the bias-corrected MS estimates using optimal coefficients that are inversely proportional to the error variance of each source (Huffman et al. 1995). An 8.5-yr analysis of global monthly precipitation based on this algorithm has been constructed and published for the period from July 1987 to December 1995 (Huffman et al. 1997) and is used by the Global Precipitation Climatology Project (GPCP; Arkin and Xie 1994) as its official final product.

Another approach to this problem is that of Xie and Arkin (1996), in which gauge observations, three kinds of satellite estimates (based on IR, MW scattering, and MW emission methods), and numerical model predictions are merged in two steps. First, to reduce the random error, the satellite estimates and the model predictions are combined linearly through the maximum likelihood estimation method, in which the weighting coefficients are inversely proportional to the error variance for the individual data source. Each of the included datasets has some characteristic that makes it likely that it adds information to the combination. The IR estimates are based on more frequent sampling than the others, the microwave estimates are based on observations of raindrops and ice particles, rather than cloud tops, and the model predictions incorporate information on atmospheric mass and motion. In principal, the linear combination of these datasets will have smaller random errors than any of them individually. Any bias in the individual datasets, however, remains in the combination. To remove that bias, the output of the first step is then blended with the gauge observations using the method of Reynolds (1988), in which the gauge data and the first-step-output are used to define the amplitude and the relative distribution, or "shape," of the precipitation field, respectively. Sensitivity tests showed that the quality of the merged analysis has been improved substantially compared to the individual data sources, with random error reduced significantly and bias removed almost completely (Xie and Arkin 1996). A comprehensive intercomparison conducted recently by Adler et al. (1996) as a part of the NASA WetNet project (Dodge 1994) found that the merged analyses of Xie and Arkin (1996) and Huffman et al. (1997) performed best in representing large-scale precipitation among over 30 participating products based on one or a combination of various information sources.

The GPCP analysis of Huffman et al. (1997) rely upon estimates based on satellite observations that are not generally available for the period before 1986, for the GPI, and mid-1987, for the microwave-based estimates. Many applications of the global precipitation datasets in climate analysis, model validation, and hydrological research, however, call for longer periods of record beginning from 1979 or earlier (Gates 1992; Schubert et al. 1993; Kalney et al. 1996), and the GPCP is investigating methods of producing such datasets. In this paper, we describe an experimental extension of the merged analysis of Xie and Arkin (1996) to cover the period from 1979 to 1995, both to

investigate the problems involved in making such an extension, and to provide users with a product better suited to diagnostic analyses for this entire period than any previously available. The lessons learned in the production of this dataset, and through its use in diagnostic studies, will increase the chances of a successful extension of the official GPCP product to cover this period.

To make possible the extension of our merged analysis, other satellite estimates of reasonable quality must be found. Recently, Xie and Arkin (1997) developed a new technique, which they called the outgoing longwave radiation (OLR)-based Precipitation Index (OPI), to estimate global monthly precipitation from the satellite-observed OLR data that are available from June 1974 to the present, except for a 10-month missing period from March to December 1978. Estimates based on the new technique are able to provide nearly complete global coverage of large-scale precipitation with high quality for most areas over the globe and for all seasons. Together with the gauge-based analysis of Xie et al. (1996) over land and the oceanic estimates of Spencer (1993) based on observations from the Microwave Sounding Unit (MSU), estimates based on the OPI technique provide a useful means to quantitatively describe the global distributions of large-scale precipitation continuously for an extended period from 1979 to the present.

In this paper, we describe a time series of global monthly precipitation analyses on a 2.5° latitude–longitude grid for the 17-yr period from 1979 to 1995 and some of its applications in the analysis of annual and interannual variability in large-scale precipitation. This analysis was produced by merging gauge observations, a number of satellite estimates, including the IR-based GPI, OLR-based OPI, MSU-based Spencer, MW-scattering-based NOAA/NESDIS (Grody 1991; Ferraro et al. 1994) and the MW-emission-based Chang (Wilheit et al. 1991), and precipitation forecasts from the NCEP–NCAR reanalysis (Kalnay et al. 1996). Section 2 describes the merging algorithm and the individual input datasets, section 3 shows results of examinations and comparisons of the analysis, section 4 presents some diagnostic results derived from the 17-yr time series, and summary and conclusions are given in section 5.

2. Methodology and data sources

a. Merging algorithm

The algorithm of Xie and Arkin (1996) is designed to construct global monthly precipitation analyses with complete coverage and improved quality by merging several kinds of individual data sources with different characteristics. The merging of the individual data sources is conducted in two steps. First, to reduce the random error, the satellite estimates and the model outputs are combined linearly through the maximum likelihood estimation method, in which the linear combination coefficients are inversely proportional to the squares of the local random error of the individual data sources. Over the global land areas, the individual random error is defined for each grid and for each month by comparing the data source with the concurrent gauge-based analysis over the surrounding areas, while over global oceanic areas it is defined by comparison with the atoll gauge data (Morrissey and Greene 1991) over the Tropics and by subjective assumption regarding the error structures over the extratropics.

Since the output of the first step contains bias passed through from the individual input data sources, a second step is included to remove it. For that purpose, the gauge-based analysis is combined with the output of the first step. Over land areas, the gauge data and the first-step-output are blended through the method of Reynolds (1988), in which the first-step-output and the gauge data are used to define the relative distribution (or "shape") and the amplitude of the precipitation field, respectively. Over the oceans, the bias remaining in the first-step-output is removed by comparison with the atoll gauge data over the Tropics and by subjective assumption regarding the bias structure over the extratropics. Since all of the atoll gauges are located over the western Pacific and the bias structure for the first-step-output over there may differ from that over other tropical and extratropical oceanic areas, uncertainty remains in the bias of the final product. However, comparisons with independent gauge observations made on the atoll of Diego Garcia (7.2°S, 72.4°E) showed only small bias over Indian Ocean (D. Stephenson 1997, personal communication).

b. Individual data sources

The major existing sources of large-scale precipitation data can be divided into seven categories based on the characteristics of the observational data used in their definitions: gauge observations, estimates inferred from satellite observations, including infrared (IR), outgoing longwave radiation (OLR), Microwave Sounding Unit (MSU), and microwave (MW) scatter-

ing and emission from the SSM/I, and the precipitation forecast by numerical models. Since different data sources based on the same observational data yield similar precipitation distributions and inclusion of additional sources with the same characteristics is unlikely to improve the quality of the merged analysis significantly (Xie and Arkin 1995), one product is selected from each of the seven categories and used as the input to the merging algorithm. In this study, the gauge-based monthly analysis produced by the Global Precipitation Climatology Centre (GPCC; Rudolf et al. 1994), the IR-based GPI (Arkin and Meisner 1987), the OLR-based OPI (Xie and Arkin 1997), the MSU-based Spencer (Spencer 1993), the SSM/I-scattering-based NOAA/NESDIS (Grody 1991; Ferraro et al. 1994), the SSM/I-emission-based Chang (Wilheit et al. 1991), and the precipitation distributions from the NCEP–NCAR reanalysis (Kalnay et al. 1996) are selected to represent each category. Figure 1 shows the temporal availability of these data sources.

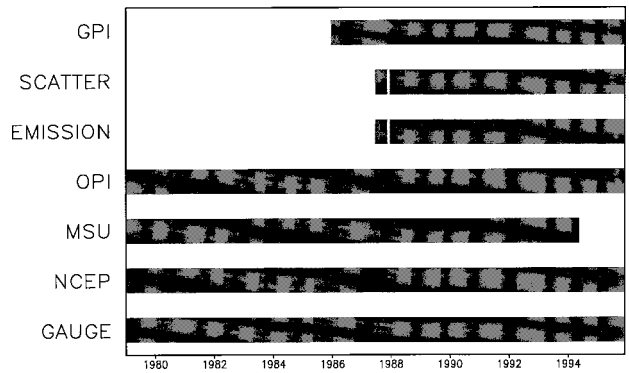

FIG. 1. Availability of the individual data sources used in the merged analysis of global precipitation.

The GPCC gauge-based analysis is constructed by interpolating quality-controlled observations from over 6700 stations globally using the spherical version of the Shepard (1968) scheme (Rudolf et al. 1994). In addition to the monthly precipitation, the number of gauges available in each 2.5° lat–long grid box is also included in the dataset. As of December 1996, the GPCC analysis is available over global land areas for the period from 1986 to 1995. The gauge-based analysis of Xie et al. (1996) is used to complete the period from 1979 to 1985. That analysis is constructed by interpolating station observations of monthly precipitation for over 6000 gauges collected in the Climate Anomaly Monitoring system (CAMS) of the NOAA Climate Prediction Center (CPC) (Ropelewski et al. 1984) and in the Global Historical Climatology Network (GHCN) of the DOE Carbon Dioxide Information Analysis Center (CDIAC) (Vose et al. 1992) using the same algorithm as used by the GPCC. Comparisons showed that the two kinds of gauge-based analysis agree very well over most global land areas (Xie et al. 1996). The quality of the gauge-based analysis depends primarily on the gauge network density. Previous studies (e.g., Rudolf et al. 1994; Xie and Arkin 1995; Xie et al. 1996) showed that the random error of the gauge-based analysis decreases with increasing gauge network density, while significant bias exists over grid boxes without gauges, where values are determined by interpolating observations over the surrounding areas. At present, nearly half of the 2.5° lat–long grid boxes over the global land areas have no gauge coverage, while fewer than 20% of them contain 5 or more gauges in the GPCC and Xie et al. (1996) gauge datasets. Intensive efforts are being made by the GPCC to collect and use gauge observations from over 35 000 stations worldwide, and improvements are expected in the quality of the gauge-based analysis.

As the GPCC and the Xie et al. (1996) analyses do not cover the oceans, the atoll gauge rainfall data of Morrissey and Greene (1991) are used to define the error structures of the satellite estimates and the model outputs over tropical oceanic areas. The atoll gauge dataset consists of monthly station observations from over 100 gauges located on atolls and small islands without high terrain. Monthly mean precipitation is calculated for 2.5° lat–long grid areas with at least one atoll gauge and used in this study. As shown in Fig. 1 in Xie and Arkin (1995), these atoll gauges are mainly located in the western Pacific along a northwest to southeast axis extending from 10°N and 140°E to 20°S and 140°W. The number of gauges available in each 2.5° lat–long grid box varies from 1 to 8, with an average of 2–3.

The GPI technique estimates area mean precipitation from fractional coverage of clouds colder than 235 K in IR images using an empirical linear relation obtained from satellite and radar observations during the GARP Atlantic Tropical Experiment (Arkin 1979; Richards and Arkin 1981). In general, the GPI is good at estimating area mean precipitation associated with deep convection, while it is incapable of detecting precipitation from clouds with warm tops and tends to misclassify thick cirrus as precipitating cloud. Overall, the GPI estimates present excellent distribution patterns of large-scale precipitation, with modest bias

over tropical oceanic areas and significant positive bias over tropical and subtropical land areas (Janowiak 1992; Arkin and Xie 1994; Arkin et al. 1994; Xie and Arkin 1995; Adler et al. 1996). The GPI estimates are produced routinely by the Global Precipitation Climatology Project (Arkin and Xie 1994) and are available from 40°S to 40°N over both land and ocean for the period from 1986 to 1995 (Arkin et al. 1994; Joyce and Arkin 1997).

The NOAA/NESDIS estimates (Grody 1991; Ferraro et al. 1994; Weng et al. 1994) are derived from the MW scattering signal of ice particles and large water drops observed from the SSM/I. After the nonraining and indeterminate pixels are eliminated by a variety of tests based on information from various channels, a scattering index (SI) is computed from the brightness temperatures in several channels and is converted into a rain rate using an empirical relation derived by comparison with radar observations over Japan. For the period from July 1990 to December 1991, when the 85V GHz channel was not available, data from 37V GHz are used instead to retrieve the scattering signals (Ferraro and Marks 1995). Generally speaking, the scattering-based technique exhibits high skill in retrieving precipitation associated with deep convection but is poor at detecting precipitation from clouds with no ice particles or large water droplets. No estimates can be made when snow or ice appear on the underlying surface, and the quality of the precipitation estimates is therefore degraded over mid- and high-latitude land areas during winter and early spring. The NOAA/NESDIS estimates are available from 60°S to 60°N over both land and ocean and cover the period from July 1987 to December 1995, with data for December 1987 missing.

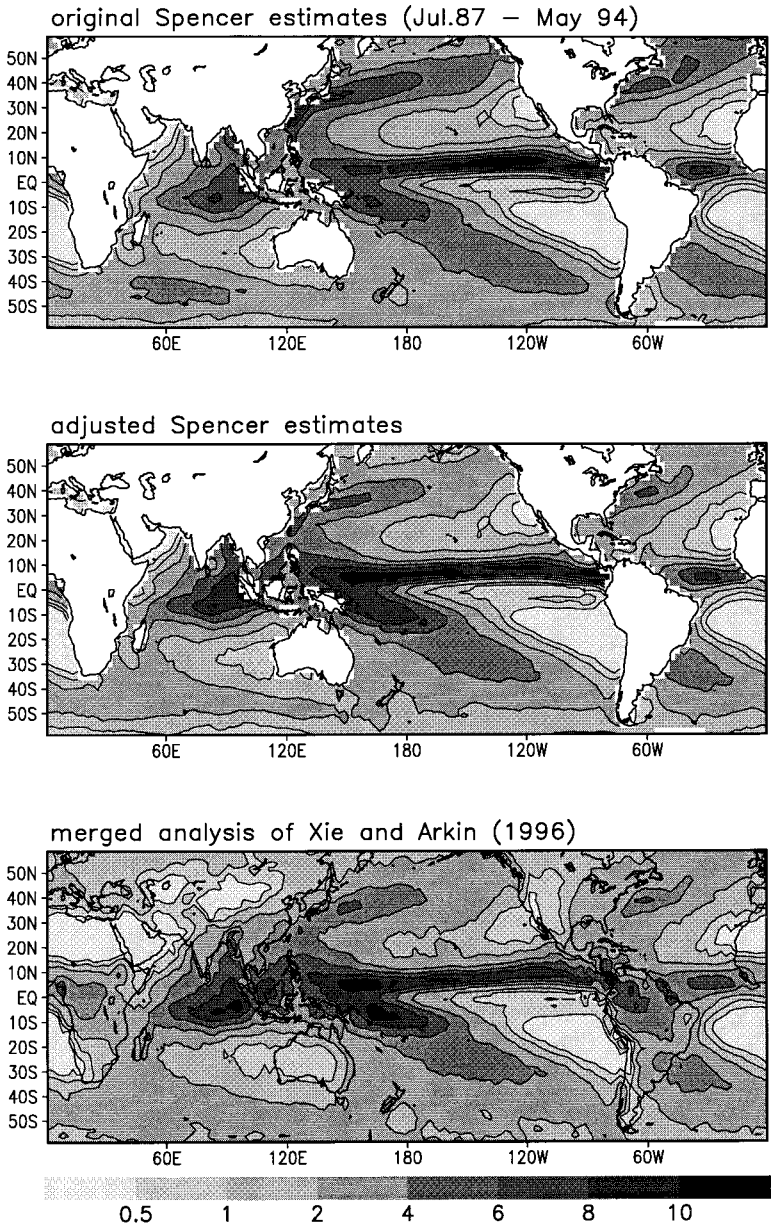

FIG. 2. Mean precipitation (mm day^{-1}) for the period from July 1987 to May 1994 from the original Spencer estimates (top), the adjusted Spencer estimates (middle), and the base product of the merged analysis of Xie and Arkin (1996) (bottom).

The Chang estimates (Wilheit et al. 1991; Chiu et al. 1993; Chang et al. 1995) are produced by retrieving precipitation information from thermal emission of liquid water as observed by the SSM/I. The histogram of a linear combination of the 19V and 22V GHz channels is computed for the target area from the observations and from a radiation transfer model using various combinations of parameters for clouds and rain rates. The parameters that result in the best match with observations are then used to calculate the rainfall estimates for the area. While the Chang estimates are derived from observations related most directly to the precipitation, they appear noisier than other estimates, probably because of the lower resolution and poor spatial sampling from the SSM/I 19V and 22V channels. The Chang estimates are available over oce-

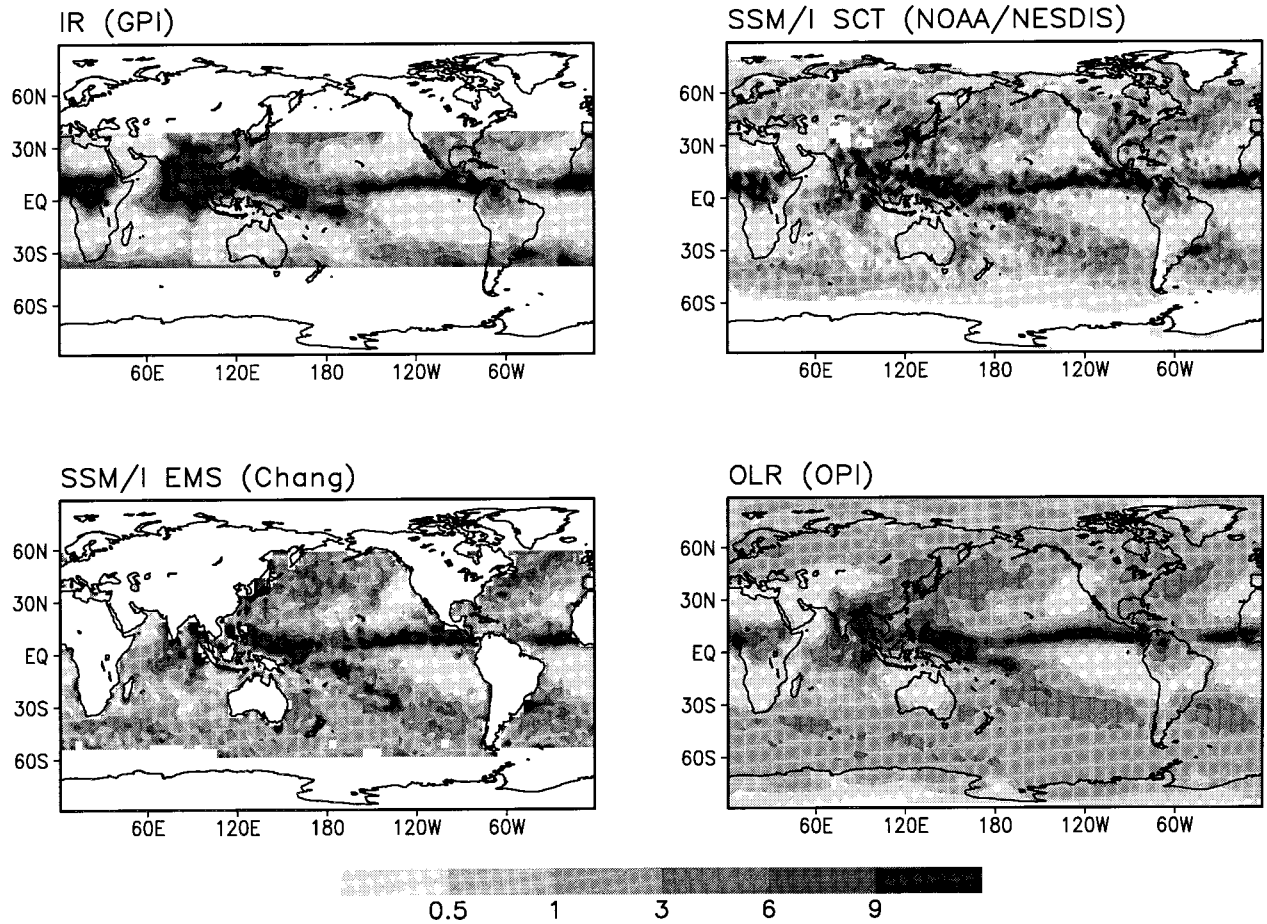

FIG. 3. Global precipitation distributions (mm day^{-1}) for August 1987 from the satellite-derived GPI, Grody, Chang, and OPI estimates.

anic areas from 60°S to 60°N for the period from July 1987 to December 1988, with estimates for December 1987 missing. Both the NOAA/NESDIS and the Chang estimates are produced using observations from a single SSM/I platform. Improvements are expected in these estimates by using both of the available SSM/I satellites when two are available.

Since none of the observational data sources is able to monitor precipitation with reasonable quality over mid- and high-latitude oceanic areas, precipitation distributions produced by numerical models are included to ensure full global coverage of precipitation. The model-produced precipitation data used in this study is that from the NCEP–NCAR reanalysis, which is defined by assimilating quality-controlled observations from all possible sources using the same global model for the entire 40-yr period from 1957 to 1996 (Kalnay et al. 1996). The monthly precipitation data used in this study covers the entire globe and extends from 1979 to 1995.

The merged analysis using the five kinds of individual data sources described above has proved to be able to provide the distribution of precipitation for the globe with high quality (Xie and Arkin 1996; Adler et al. 1996). However, the GPI and the SSM/I-based estimates are not available for most of the period from 1979 to mid-1987. To facilitate the extension of the merged analysis, it is necessary to find other satellite-based estimates of precipitation with extended availability and reasonable quality. Although many sorts of observations are available from various meteorological satellites since the beginning of the 1970s, only the emission data from the MSU and the OLR data from the Advanced Very High Resolution Radiometer (AVHRR) provide continuous temporal coverage with useful information from which large-scale precipitation estimates can be made.

The MSU-based precipitation data used here are based on the monthly estimates of Spencer (1993), which cover the global oceans from 60°S to 60°N and extend from January 1979 to May 1994. A precipitation index is first calculated from the anomalous tem-

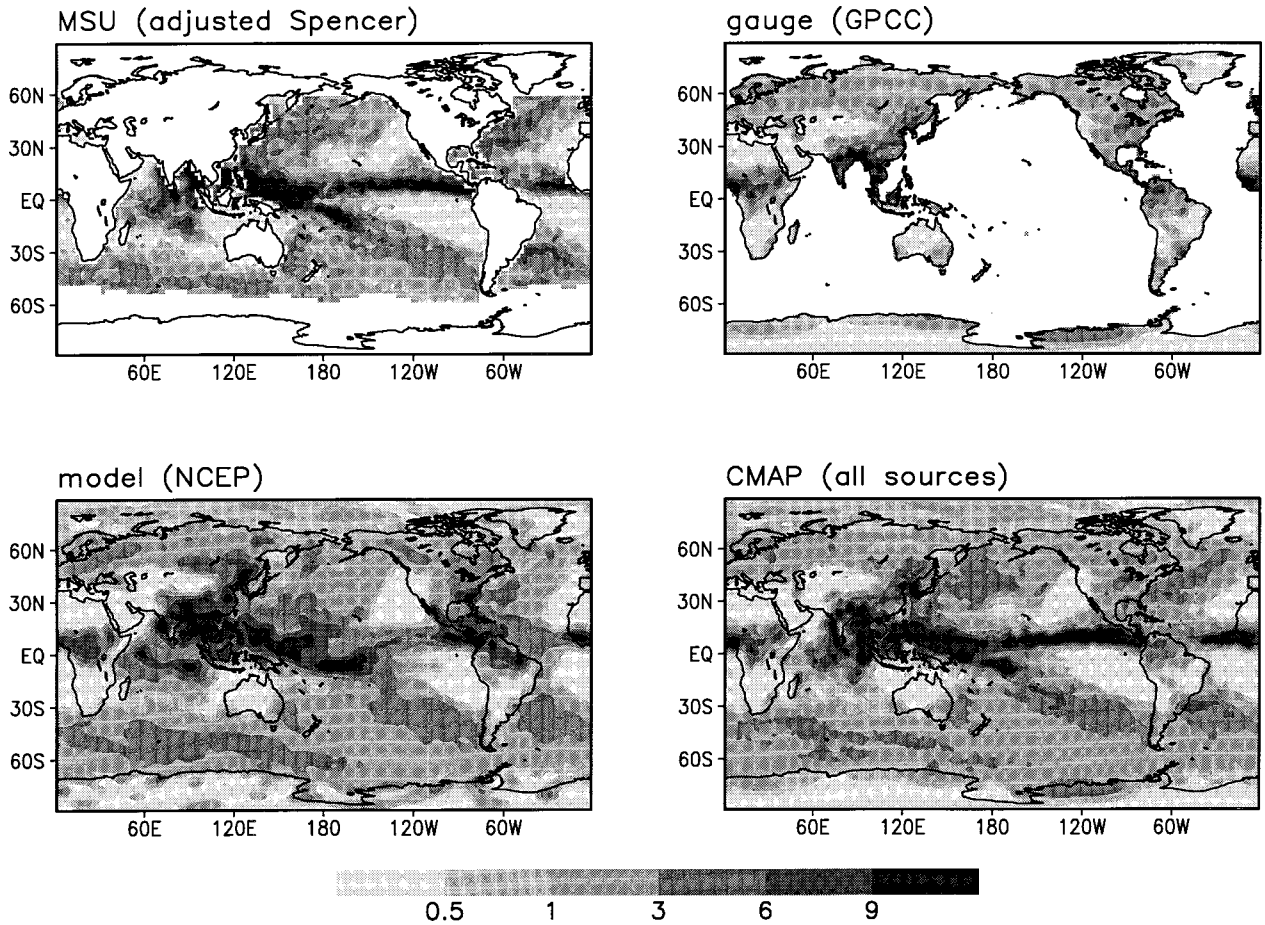

FIG. 4. Global precipitation distributions (mm day^{-1}) for August 1987 from the adjusted Spencer estimates (MSU-R), the gauge-based analysis of the GPCC, the NCEP–NCAR reanalysis, and the CMAP.

perature elevation in MSU channel 1 (50.3 GHz), where warming is mainly due to the thermal emission by liquid water. This index is then calibrated into rainfall using observations from over 100 coastal and atoll gauges around the globe. The spatial distribution of the Spencer precipitation index, however, exhibits two major systematic differences from estimates based on the SSM/I and the GPI. The Pacific intertropical convergence zone (ITCZ) is characterized by a precipitation maximum over the eastern Pacific in the Spencer estimates, while it has its maximum over the western Pacific warm pool coupled with a minimum over the central Pacific in the GPI and most SSM/I-based estimates (Janowiak et al. 1995; Adler et al. 1996). In addition, the midlatitude storm tracks are much stronger in the Spencer estimates than in other estimates. No conclusions regarding the relative quantitative accuracies of the various estimates can be made, because of the lack of direct precipitation measurements over the oceanic areas in question. However, this systematic differences between the MSU and the other sources would result in an undesirable temporal discontinuity in the merged analysis. Adjustments to the various sources are therefore needed to ensure that artifacts in the form of spatial or temporal discontinuities do not degrade the utility of the merged analysis.

For that purpose, a special dataset of global monthly precipitation is created by merging the gauge observations of the GPCC, the satellite estimates of the GPI, NOAA/NESDIS, and the Chang, and the NCEP–NCAR reanalysis for the 8-yr period from July 1987 to June 1995. The merged analysis for this 8-yr period, called base product, is then used to adjust the original Spencer estimates as follows. First, the mean annual cycle is calculated for both the Spencer estimates and the base product for each grid box using data for the period from July 1987 to May 1994 when both are available. The adjustment factor is then defined for each grid box and for each calendar month as the ratio of the local mean of the base product over

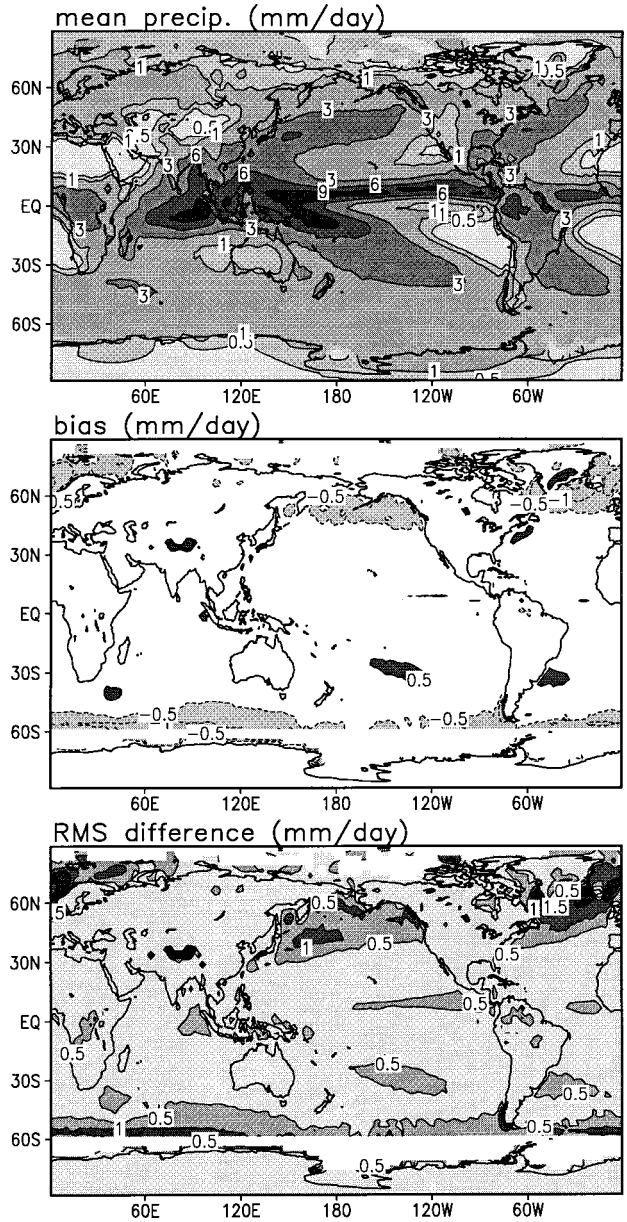

FIG. 5. Distributions of the mean precipitation (top; mm day^{-1}) for the 17-yr period from 1979 to 1995 from the CMAP using all sources and its bias (middle; mm day^{-1}) and rms difference (bottom; mm day^{-1}) compared to the observation-only version of the CMAP. Areas with more (less) precipitation observed in the observation-only version, with differences larger than ±0.5 mm day^{-1}, are indicated by heavy (light) shading in the bias map.

a 9×9 grid array centered at the target to that of the Spencer estimates, with its value limited to a range of 0.5–2.0. The original Spencer estimates for the entire period from January 1979 to May 1994 are finally modified month by month by multiplying with the adjustment factor appropriate for the grid box and for the month, resulting in the dataset, which we will refer to as the MSU-R, used in this study. This process retains the temporal and spatial variability during the period while constraining the large-scale features of the Spencer estimates to match the combination of the recent data sources (Fig. 2). However, some differences between the MSU-R (middle) and the base product (bottom) are found in smaller-scale features, probably because of year-to-year variations in the position of rainbands associated with the storms tracks and oceanic convergence zones.

The other satellite estimate that is available for the entire 17-yr period is the OPI, which is based on the findings that the anomaly of precipitation correlates well with that of OLR over most of the globe and that the proportional coefficient relating them can be expressed with high accuracy as a linear function of the local mean precipitation (Xie and Arkin 1997). The OPI estimates monthly precipitation for a grid area in three steps. First, the mean annual cycle of precipitation is obtained, and the precipitation anomaly is estimated from the OLR anomaly using the coefficient appropriate for the mean precipitation at each location and for each calendar month. The total precipitation is finally estimated as the sum of the mean annual cycle and the anomaly. The process requires a base period for which the mean annual cycle of precipitation is known; in the present study, the merged analysis for the 8-yr base period from July 1987 to June 1995 is used. The OPI estimates are available for the entire globe and for the entire 17-yr period.

c. Merged analysis

A monthly precipitation analysis is then constructed for the 17-yr period from January 1979 to December 1995 by merging the seven kinds of individual data sources, whenever available, using the algorithm of Xie and Arkin (1996). For convenience, hereafter we will call this dataset of global monthly precipitation the CPC Merged Analysis of Precipitation (CMAP). Figures 3 and 4 show the distributions of global precipitation for August 1987 from the individual data sources and from the CMAP. All of the individual data sources exhibit similar patterns of large-scale precipitation distribution, but with differences in smaller-scale features and in amplitudes. The GPI contains larger values over extratropical areas, and the NOAA/NESDIS, Chang, and MSU-R estimates, which are based on fewer temporal samples, exhibit considerable local variation, while the distributions of the GPI, OPI, and reanalysis are smoother. The merged analysis attempts to take advantage of each individual

source, with patterns determined by the combination of satellite estimates and model outputs and amplitude defined by the gauge observations.

Since global precipitation distributions are often used to verify simulations and predictions from numerical models of the atmosphere, a version of the CMAP that is based only on observations, and thus can be used for independent comparisons with model-based products, is required. At the same time, complete global fields of precipitation, which are not obtainable without the use of model forecasts, are needed for many other purposes, such as diagnostic analyses of the global hydrological cycle. The merging algorithm of Xie and Arkin (1996) was used to create an observation-only version of the CMAP by dropping the NCEP–NCAR reanalysis dataset and using only the six observation-based data sources. (This same process could be applied to any one, or combination, of the input datasets to create an analysis that did not use, for example, estimates based on SSM/I observations. However, we are not aware of any pressing requirement for other versions, and so only the "all-sources" and "observation-only" versions were constructed.) The OPI and the MSU-R are redefined by using the base product merged from GPCC gauge data and satellite estimates of the GPI, NOAA/NESDIS, and Chang to ensure that the no-model version of the merged analysis is completely independent of the model results. We will refer to the observation-only product as the CMAP/O. To examine the differences between the two versions of the merged analysis, comparisons are conducted between the CMAP and CMAP/O. Shown in Fig. 5 are the mean distribution of the CMAP using all sources and its bias and rms difference relative to the CMAP/O for the 17-yr period from 1979 to 1995. No satellite estimates are available with reasonable quality over oceanic areas poleward of 60°S/N. The largest differences between the CMAP and the CMAP/O are observed in the midlatitude oceanic storm tracks, where significant differences in precipitation exist between the satellite estimates and the reanalysis. Some differences are also found in the tropical oceanic convergence zones, but with substantially smaller magnitude relative to the local mean precipitation. Over land areas, the two versions of the CMAP are identical over grid areas with one or more gauges and are very close over most other grid areas.

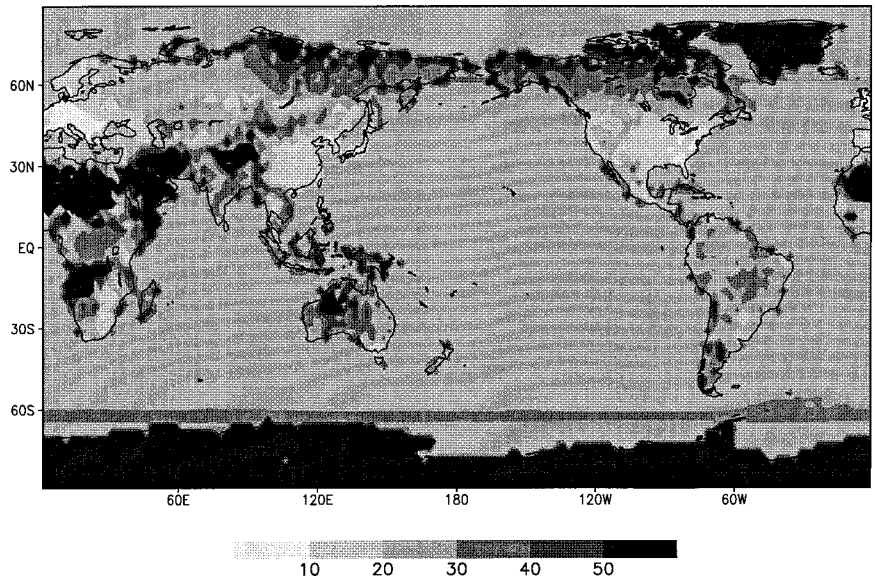

FIG. 6. Distribution of the estimated error (percentage of the mean) for the monthly analysis averaged over the 17-yr period.

In addition to the monthly value of precipitation, relative error for each 2.5°lat–long grid area is estimated using the method described in Xie and Arkin (1996) and included in the 17-yr dataset as an index of the quality of the merged analysis. Over the so-called anchor grid areas, where the merged analysis is defined to have the same value as that in the gauge-based analysis, the relative error is defined as the spatial sampling error of the gauge observations, which is assumed to be a function of the density of the local gauge network. Over other grid areas, including all oceanic areas and land areas with no gauge coverage, the error is estimated as the expectation of the random error of the first-step-output, which is a linear combination of several individual sources with weights based on the random errors of each. Xie and Arkin (1996) showed that the relative error estimated in this manner agreed very well with that calculated by comparing with independent observations over land areas. Over oceanic areas, where no additional data are available to verify the various assumptions involved in the definition of the relative error, the accuracy of this field is less certain. More work is needed to further our understanding of the error structures of the individual data sources and to improve the quantitative es-

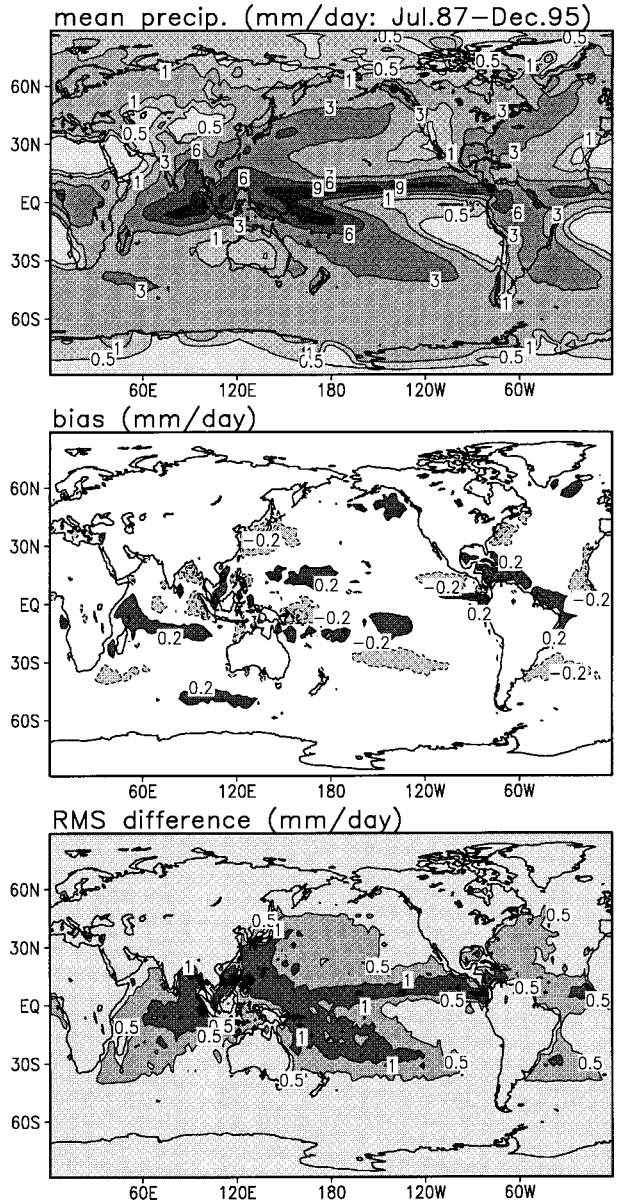

FIG. 7. Distributions of the mean precipitation (top; mm day^{-1}) for the period from July 1987 to December 1995 from the CMAP and its bias (middle; mm day^{-1}) and rms difference (bottom; mm day^{-1}) from the version excluding the GPI and the SSM/I-based estimates. Areas with more (less) precipitation observed in the version excluding the GPI (SSM/I) estimates, with differences larger than 0.2 mm day^{-1}, are indicated by heavy (light) shading in the bias map.

timation of the relative error of the CMAP over oceanic areas (Oki and Sumi 1994; Huffman 1997).

Figure 6 shows the distribution of the estimated error, relative to the mean, for monthly precipitation averaged over the 17-yr period. Relatively small errors are observed over most populated land areas in western Europe, China, and North America, while relatively large errors are found over desert areas and the polar caps, where light precipitation is observed by sparse gauge networks. Over the oceans, only a crude estimate based on subjective assumptions regarding the error structures for the individual data sources is available, and the results therefore can be only used as indexes of the relative quality of the merged analysis. This yields a smooth field with values of about 25% over the global oceanic areas from 60°S to 60°N and around 30% polarward where only OPI and model outputs are available. Unlike the error fields presented by Huffman et al. (1997), no contribution from sampling error is explicitly included here.

3. Investigation

a. Temporal continuity and spatial coherence

One potential shortcoming of the 17-yr CMAP results from the use of different individual data sources for the different periods. As shown in Fig. 1, only four kinds of data (gauge, MSU-R, OPI, and reanalysis) are available during the early part of the period from January 1979 to December 1985, while all of the seven data sources are used for the period following July 1987. In particular, the absence of the SSM/I-based estimates, which play an important role in defining the analysis over global oceanic areas, might result in significant artifacts in the spatial distribution patterns and temporal variations depicted by the dataset.

Two experiments are conducted to examine the possible systematic differences in the spatial distributions and the discontinuity in time series. First, a variation of the CMAP is constructed for the period from July 1987 to December 1995 by using only the gauge observations, OPI and MSU-R estimates, and the NCEP–NCAR reanalysis. The results are then compared to the version of CMAP that uses all seven data sources for the same period to investigate the impact of the estimates based on GPI and SSM/I observations.

Figure 7 shows the distribution of the mean precipitation for the period as obtained from the all-sources version of the CMAP (top) and its bias (middle) and rms difference (bottom) compared to the version without the GPI and the SSM/I-based estimates. No significant differences are observed over the global land areas where precipitation distribution is determined mainly by the gauge observations. Over oceanic areas, the bias is generally very small, typically less than 0.2 mm day^{-1}, while the rms difference

is about 10%–20% and exhibits a distribution pattern roughly similar to that of the total precipitation.

Figure 8 shows the time series of the mean precipitation for several latitude zones over the oceans as obtained from the CMAP based on all available sources for the entire 17-yr period (solid line) and from that using only the gauge observations, MSU-R and OPI estimates, and the NCEP reanalysis for entire period (dotted line). These time series are, of course, identical until July 1987, when the SSM/I-based estimates became available. Encouragingly, no discontinuity is observed in any of the time series around July 1987 when the data used changed. The time series for the two versions of the merged analysis exhibit the same temporal variation patterns with similar amplitudes over all of the seven zonal areas for the period from July 1987 to December 1995. The rms difference between the two versions of the CMAP (dashed line) is very small over high latitudes where reanalysis, which is used in both versions, plays a major role in determining the merged analysis, while moderate differences (~15%) are observed over the tropical oceans where the GPI and SSM/I-based estimates receive significant weights in the merging. Not shown are the time series of precipitation and differences over land areas, where the merged analysis is strongly constrained by the gauge-based analysis and the changes in satellite data availability have essentially no impact.

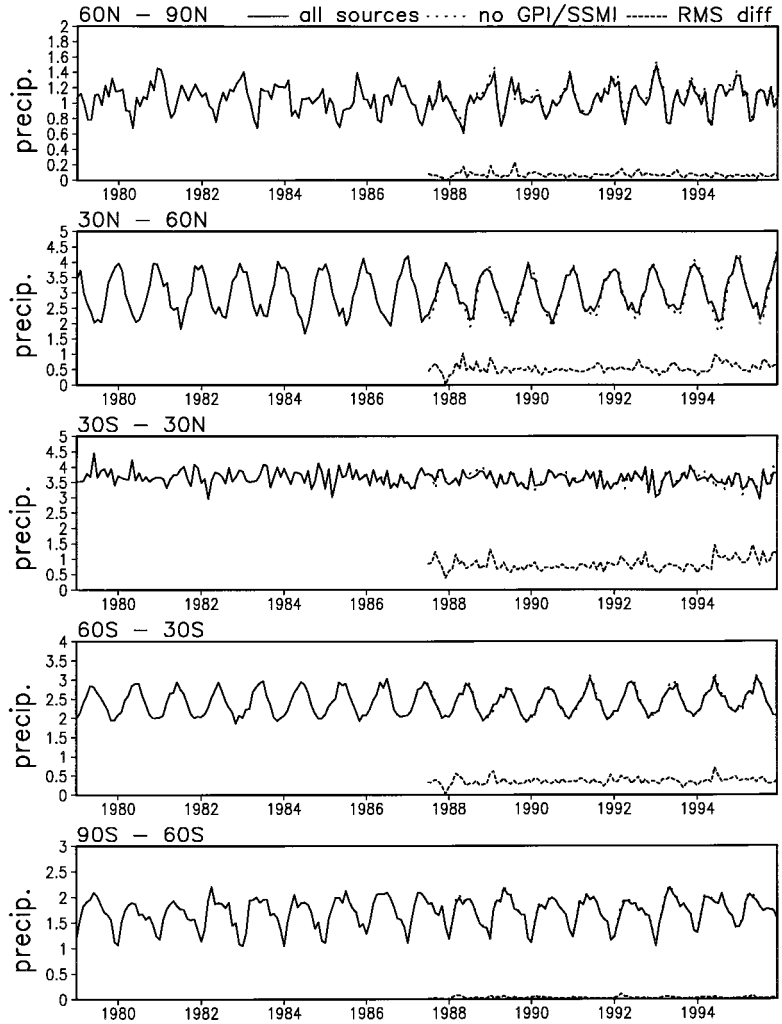

FIG. 8. Time series of the mean precipitation (mm day^{-1}) from the CMAP with all sources (solid line), CMAP with no GPI and SSM/I-based estimates (dotted line), and their rms difference (dashed line) over several oceanic zonal areas.

b. Comparison with independent gauge observations

Through cross validation and simulation tests, Xie and Arkin (1996) demonstrated that the merging algorithm used in this study is able to construct global precipitation analyses with better quality than the individual data sources used. To investigate the quantitative quality of the merged analysis, comparisons are made with a nearly independent monthly rainfall dataset, which is constructed by the GPCP Surface Reference Data Center (SRDC) by interpolating gauge observations over several selected land areas with much denser networks than that of the GPCC (McNab, http://www.ncdc.noaa.gov/ogp/papers/mcnab.html).

The SRDC monthly precipitation dataset used in this comparison covers 15 2.5°-lat–long grid areas located over five areas in Australia, Canada, Honduras, southeast United States, and Thailand, where gauge networks present relatively high density and uniform distributions (see Fig. 9 of Huffman et al. 1997). The areal mean precipitation for each grid area is calculated by an algorithm called PRISM, which is based on linear regression of gauge precipitation and terrain (Daly et al. 1994). Since the SRDC dataset is based on observations from over 10 times as many gauges as in the GPCC dataset and only a small portion of the gauges are duplicated (see Table 1 in Huffman et al. 1996), the SRDC precipitation analysis is nearly

TABLE 1. Comparisons of the SRDC gauge data with the CMAP.

		GPCC gauge number					
		0	**1**	**2**	**3**	**4**	**5+**
Bias (%)	CMAP	6.3	88.9	–3.9	1.0	–0.5	5.1
	CMAP/O	5.2	88.9	–3.9	1.0	–0.5	5.1
Rmse (%)	CMAP	74.6	123.9	19.5	16.8	18.3	25.1
	CMAP/O	75.8	123.9	19.5	16.8	18.3	25.1
Corr	CMAP	0.880	0.919	0.923	0.968	0.959	0.951
	CMAP/O	0.876	0.919	0.923	0.968	0.959	0.951

CMAP: CPC merged analysis of precipitation with all sources
CMAP/O: CPC merged analysis of precipitation—observation only

independent of the GPCC gauge-based analysis and thereby the merged analysis. Only the SRDC values for grid areas with 10 or more gauges are used in this study to ensure that the comparison results represent the quality of the merged analysis and not simply the similarity between the SRDC and GPCC datasets.

Table 1 shows the results for a 6-yr period from January 1986 to December 1991. In general, the quality of the merged analysis is very good and it improves with the increasing numbers of gauges available in the GPCC dataset. The correlation, bias, and relative random error are about 0.88, 6%, and 75% over grid areas with no GPCC gauge where the merged analysis is defined by interpolating the nearby gauge data with constraints in the "shape" of the precipitation field determined by the satellite estimates and model outputs, while they are typically over 0.9, less than 5% and 20% over grids areas with GPCC gauges where the merged analysis is defined as the same as the GPCC gauge analysis. The large bias (123%) and random error (89%) for the grid areas with one GPCC gauge come from a grid area over Thailand where significant inhomogeneity exists in precipitation distribution because of the mountainous terrain. Inclusion of more gauge observations in the GPCC analysis is desirable to improve the quality of the merged analysis over such areas. There are small increases in the relative bias and random error, and decreases in the correlation in Table 1 for grid areas with 4, or 5 or more, stations. These fluctuations, while not clearly statistically significant, appear to result from the fact that, on average, less precipitation is observed over the grid areas with more GPCC gauges. Since the fundamental random error, or noise, in the system does not decrease in proportion, this results in higher relative error and degraded correlations for the grid areas with less precipitation. Over oceanic areas, where independent observations with reasonable spatial and temporal coverage are not available, the quality of the merged analysis cannot be tested satisfactorily at this time.

c. Comparison with the merged analysis of Huffman et al. (1997)

The merged analysis described in this study is compared to that of Huffman et al. (1997) for the period from July 1987 to December 1994 when both are available. Since the merged analysis of Huffman et al. (1997) is produced from the gauge observations and the satellite estimates based on the GPI and the SSM/I observations, the observation-only (CMAP/O) version of our merged analysis is used in this comparison. Figure 9 shows the spatial distributions of the correlation (top), bias (middle), and root-mean-square difference (bottom) between the two datasets. Good agreements, characterized by high correlation, relatively small bias, and random error, are observed over global land areas where gauge data plays a major role in both of the algorithms and over tropical and subtropical oceanic areas where most satellite estimates exhibit high skills in estimating large-scale precipitation (Xie and Arkin 1995; Janowiak et

TABLE 2. Mean precipitation (mm day^{-1}).

Sources	Area	DJF	MAM	JJA	SON	Annual
CMAP	Land	1.76	1.82	2.07	1.80	1.86
(All sources)	Ocean	2.99	3.01	3.07	3.01	3.02
	Globe	2.64	2.67	2.79	2.67	2.69
Jaeger (1976)	Land	1.83	1.82	2.39	2.01	2.01
	Ocean	3.00	2.81	2.98	2.86	2.91
	Globe	2.67	2.53	2.81	2.62	2.66
Legates and	Land	1.85	1.89	2.22	1.90	1.97
Willmott (1990)	Ocean	3.67	2.51	2.85	3.57	3.15
	Globe	3.16	2.33	2.67	3.10	2.82

al. 1995). Significant differences occur over the extratropical oceans, where the analysis of Huffman et al. (1997) is defined as identical to the emission-based estimates of Chang, while, in the CMAP/O it is determined from a linear combination of the estimates from both SSM/I-based estimates, the MSU-R, and the OPI, with a bias correction based on the tropical atoll gauge observations of Morrissey and Greene (1991) and subjectively derived extrapolation to the extratropics. Some differences over land areas can be attributed to the fact that Huffman et al. (1997) correct the gauge-based analysis for systematic error caused by aerodynamic effects (Sevruk 1989), while we used the GPCC analysis in its original form. The differences observed over the oceans, meanwhile, may come from the different sources used in the analysis as well as the different ways to combine them.

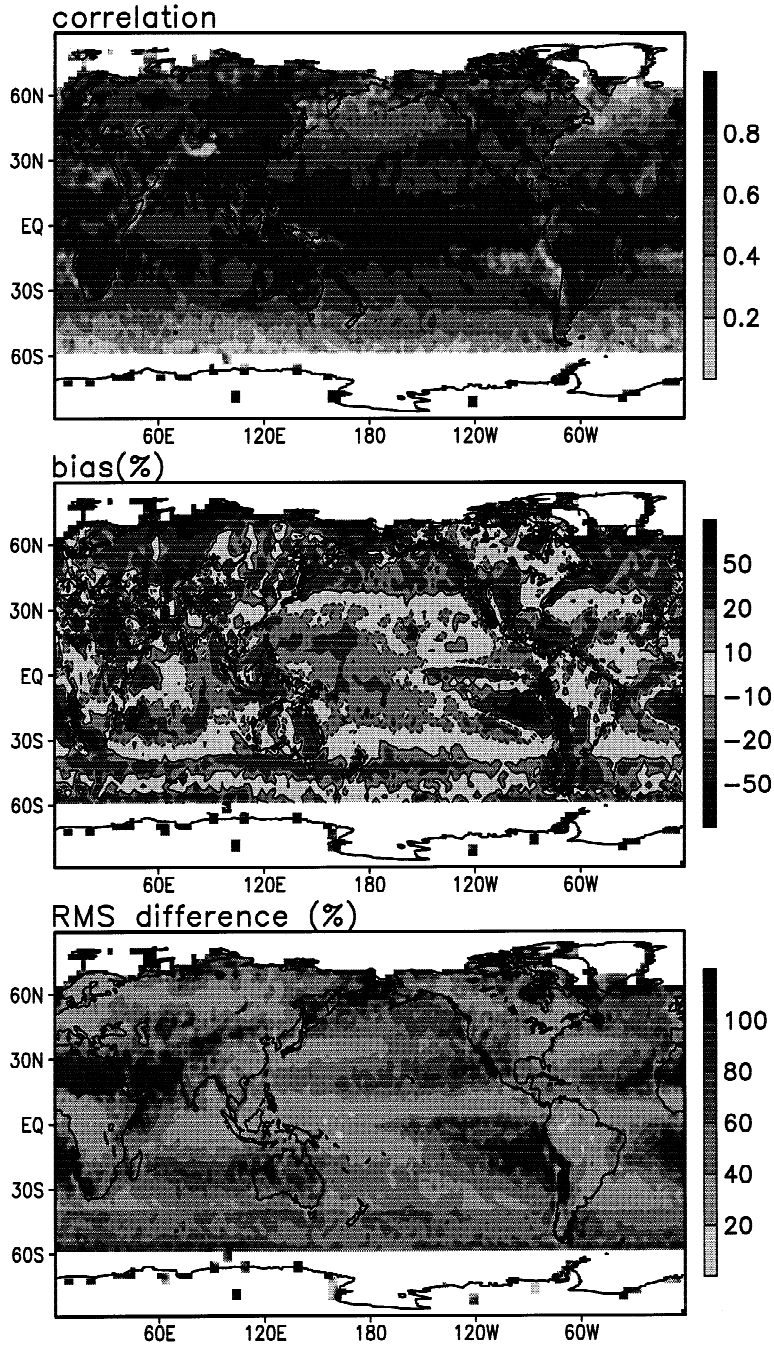

FIG. 9. Correlation (top), bias (middle), and rms difference (bottom) between the merged analysis of Huffman et al. (1997) and the CMAP for the period from July 1987 to December 1994. Both the bias and the rms difference are plotted in percentage relative to the CMAP.

4. Global precipitation

The spatial and temporal variability of global precipitation as observed in the CMAP is investigated for the 17-yr period from 1979 to 1995 and compared to the long-term means of Jaeger (1976; hereafter called J76) and Legates and Willmott (1990; hereafter called LW). Figures 10–14 present the spatial distributions of the mean precipitation as obtained from the 17-yr CMAP (top), and from the long-term means of J76 (middle) and LW (bottom) for the entire year and for the four seasons December–February (DJF), March–May (MAM), June–August (JJA), and September–November (SON), while Table 2 shows the precipitation amounts averaged over the land, the ocean, and the entire globe. Here, the land areas are defined as those 2.5° lat–long grid boxes with 50% or more land coverage.

In general, the 17-yr mean of the CMAP is in good agreements with those of J76 and LW, especially over land areas. The annual mean precipitation over the entire globe is 2.69 mm day^{-1} in the 17-yr CMAP, compared to 2.66/2.82 mm day^{-1} in J76/LW. All three datasets exhibit similar large-scale distribution patterns for the annual mean precipitation (Fig. 10), with rainbands associated with the ITCZ, the South Pacific convergence zone (SPCZ), the midlatitude oceanic storm tracks, and the tropical continental maxima. A

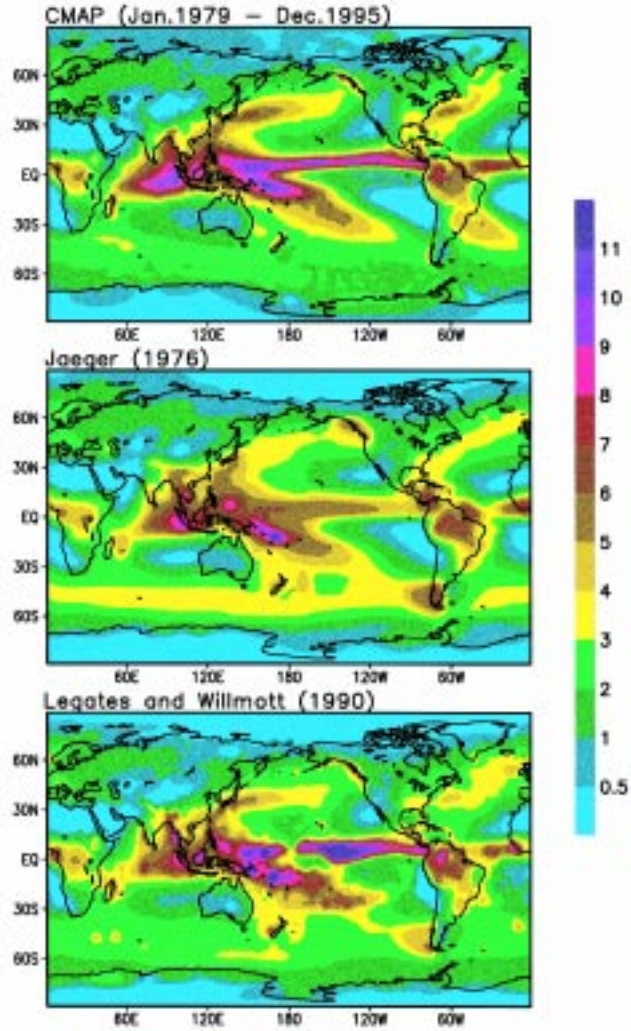

FIG. 10. Distributions of the annual mean precipitation (in mm day^{-1}) as obtained from the CMAP (top), from Jaeger (1976) (middle), and from Legates and Willmott (1990) (bottom).

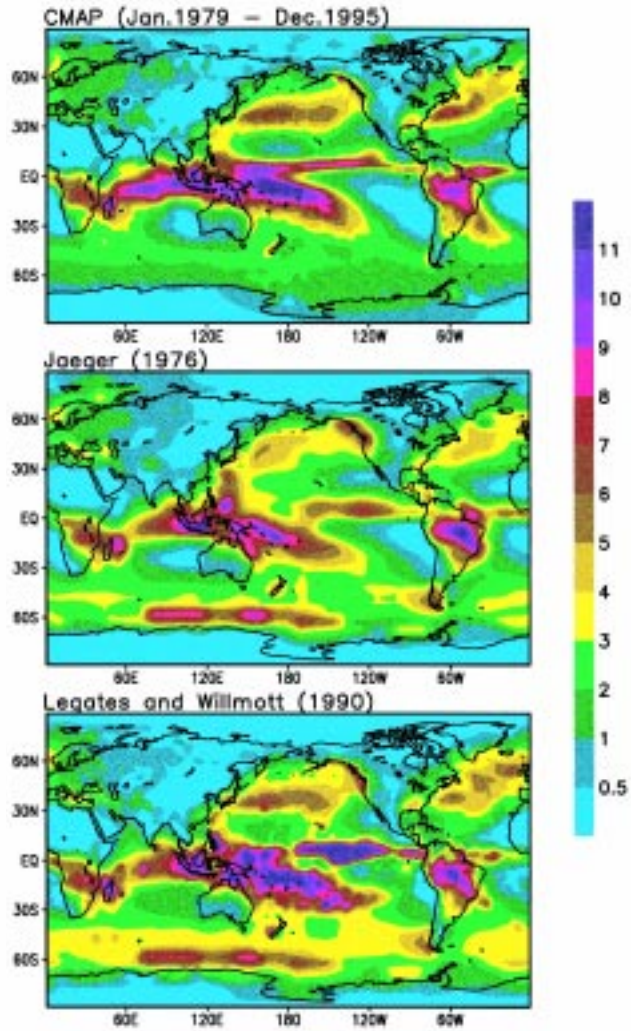

FIG. 11. As in Fig. 10 except for the December–February (DJF) mean precipitation.

gap in the ITCZ is observed over the central Pacific in the long-term mean of LW and, although not as distinct, in the 17-yr CMAP as well, while the long-term mean of J76 exhibits broader and smoother distributions for the rainbands. Major differences are observed over the eastern Pacific where only satellite-derived estimates are available. Heavy rainfall, greater that 10 mm day^{-1}, is observed in LW, while values in J76 are approximately half that. In CMAP, a well-defined ITCZ with peak values roughly midway between J76 and LW is observed.

Significant seasonal variations in global precipitation are observed in the 17-yr CMAP. During DJF (Fig. 11), the SPCZ is strong and the ITCZ is relatively weak over the central and eastern Pacific. The midlatitude storm tracks are connected with the ITCZ in the Southern Hemisphere, while they are more separated in the Northern Hemisphere. The SPCZ becomes weaker and the ITCZ intensifies over the western Pacific warm pool during MAM (Fig. 12). During JJA (Fig. 13), the SPCZ is at its weakest, while the ITCZ is strong over both the eastern and western Pacific, with a slight relative minimum observed over its central part. The precipitation distribution for the SON period (Fig. 14) is characterized by the SPCZ recovering its strength and by a moderate ITCZ with large precipitation over the central Pacific. Similar behavior is observed in J76 and LW, except that the seasonal variations of the ITCZ over the central and eastern Pacific are quite different in both phase and the amplitude. Generally speaking, J76 tends to exhibit smaller precipitation for all seasons over the eastern Pacific, while LW gives much larger values.

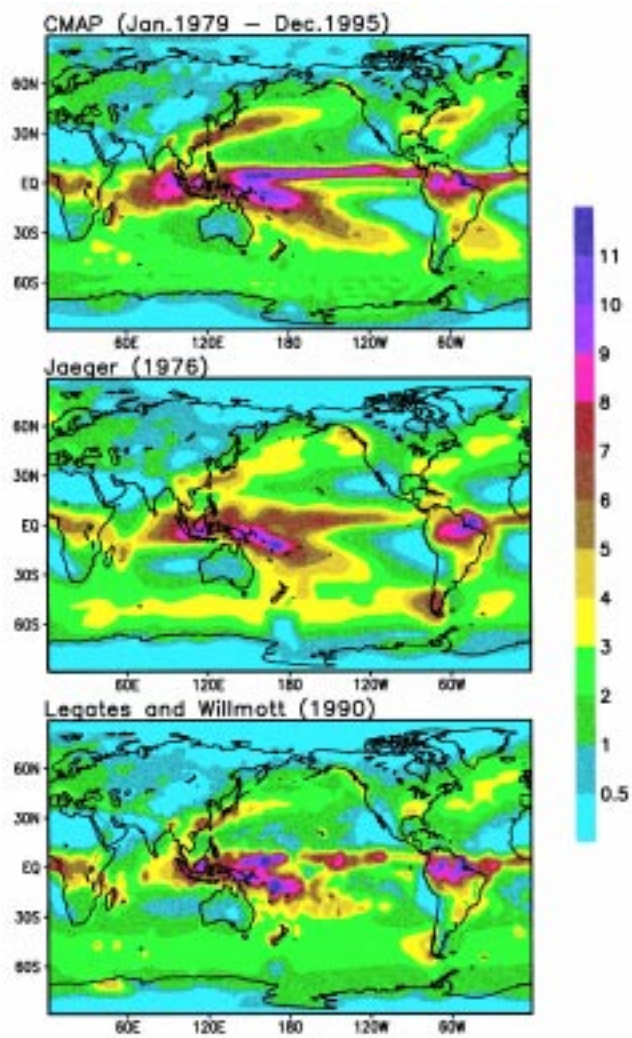

FIG. 12. As in Fig. 10 except for the March–May (MAM) mean precipitation.

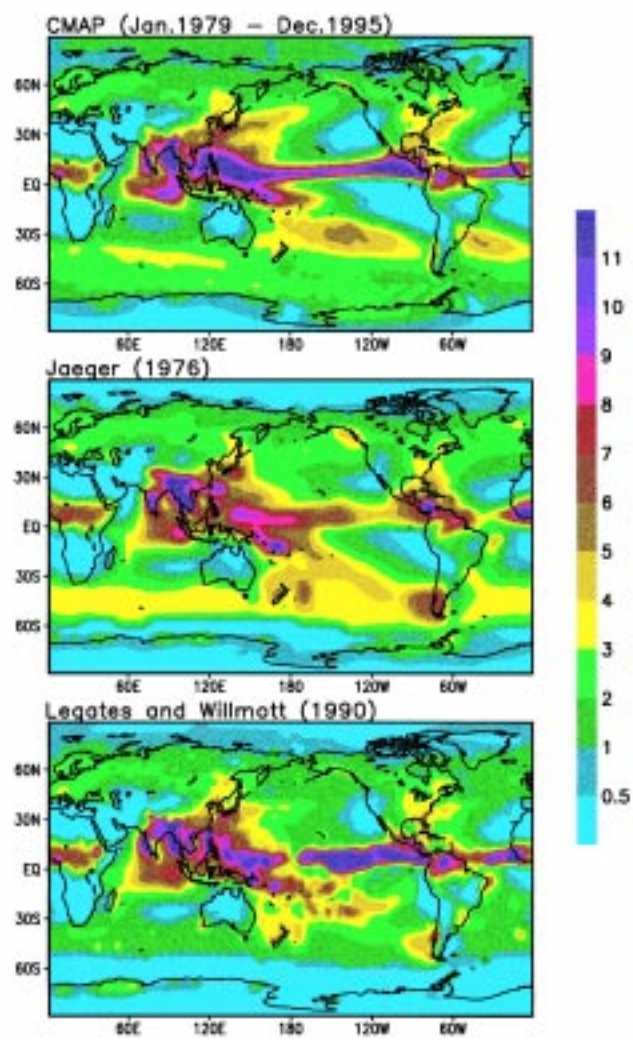

FIG. 13. As in Fig. 10 except for the June–August (JJA) mean precipitation.

Shown in Fig. 15 are the annual cycles of the precipitation averaged over land (top), over ocean (middle), and over the entire globe (bottom) as obtained from our 17-yr CMAP (open circle) and from the long-term means of J76 (open square) and LW (solid square). All of the three datasets depict similar annual cycles of precipitation over global land areas, with maxima during July–August, although the amplitude for the merged analysis is smaller than those for the two published long-term means. Over oceans, the CMAP shows little annual variability, with the highest month less than 5% above the lowest. J76 exhibits somewhat more variability, although without great regularity, with peaks in February, June, and September up to 15% greater than the monthly minima found in April and October. LW, meanwhile, presents quite a different appearance, with peak values in November more than 50% greater than the minimum in April. Secondary peaks are found in January and June, and a relative minimum occurs in August. A significant portion of these large annual variations results from changes in the large maxima over the eastern Pacific. Over the entire global area, the 17-yr CMAP exhibits a flat annual cycle, ranging from 2.62 mm day^{-1} in March to 2.81 mm day^{-1} in June.

The 17-yr CMAP is also applied to examine the interannual variability associated with the El Niño–Southern Oscillation (ENSO) phenomen. Shown in Fig. 16 are the time series of the sea surface temperature (SST) anomaly over the Niño 3 area (5°S–5°N; 150°–90°W) and a time–latitude cross section of precipitation averaged over the Pacific sector (140°E–

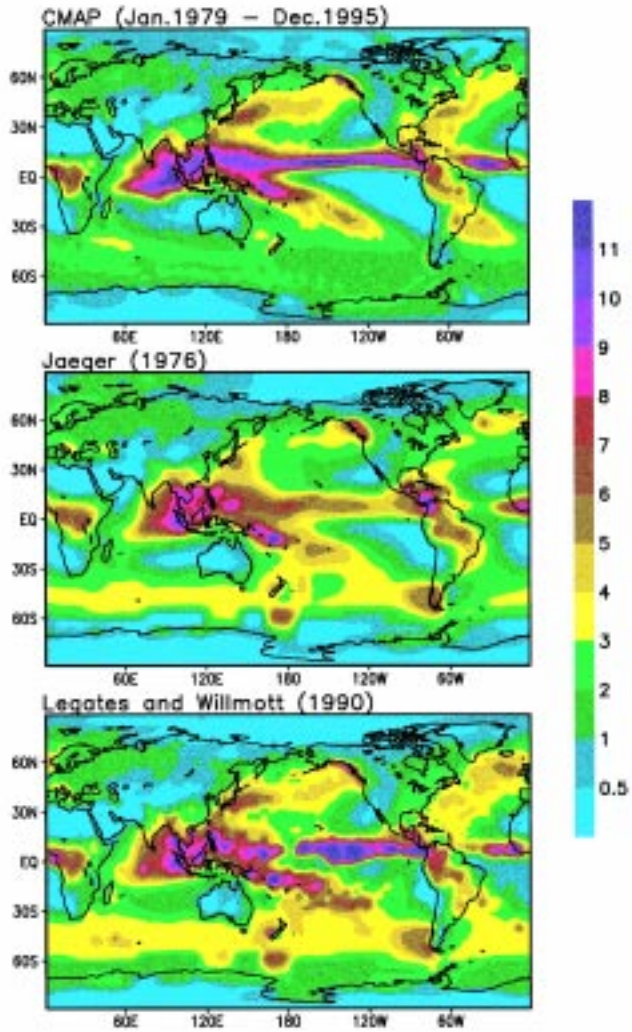

FIG. 14. As in Fig. 10 except for the September–November (SON) mean precipitation.

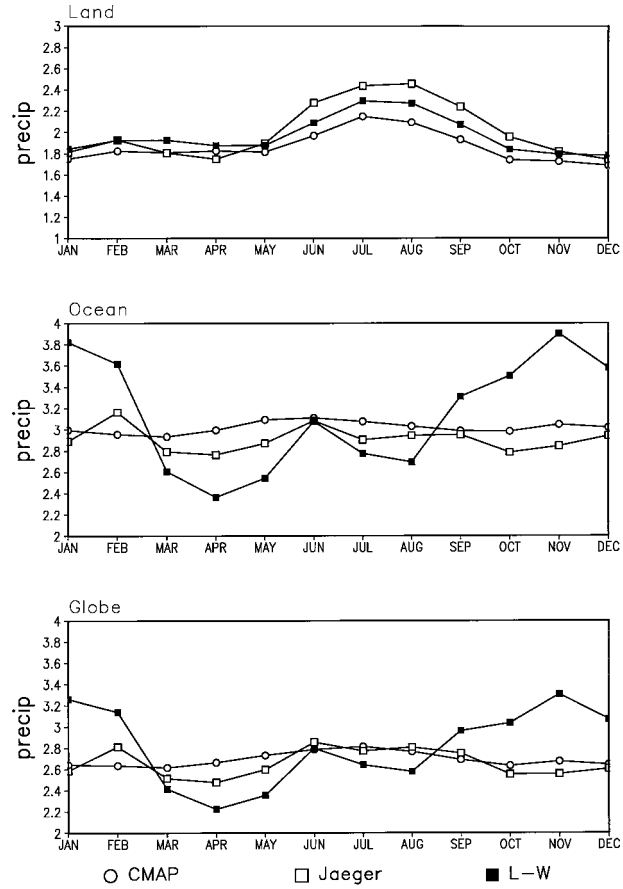

FIG. 15. Annual cycles of mean precipitation (mm day^{-1}) over land (top), ocean (middle), and the entire globe (bottom) from the 17-yr CMAP (open circle), from Jaeger (1976) (open square) and from Legates and Willmott (1990) (solid square).

60°W). A significant annual cycle is observed that is clearly modified by the SST anomaly. The magnitude of the precipitation becomes larger, and the distribution extends farther south when the SST is warmer than average, while the precipitation becomes weaker in general when the SST anomalies are negative.

Since the time–latitude cross section in Fig. 16 is not able to reveal the east–west variation in precipitation, spatial distributions are composited for warm and cold ENSO episodes, and their differences are investigated. Although there are many ways to define an ENSO episode, we adopted a rather simple and objective approach in which a cold/warm ENSO episode is declared for a season if the SST anomaly over the Niño 3 area is < –0.5°C/> 0.5°C for the period. The classification based on this method results in 3–6 ENSO events for each three-month period during the 17-yr period. Figure 17 shows the distributions of the difference observed during the warm and cold conditions (warm minus cold) for the DJF, MAM, JJA, and SON seasons.

During DJF, warm episodes are characterized by more precipitation over the central Pacific, southeastern South America, the extreme northeastern Pacific and adjacent coastal regions of North America, and over a belt extending from the eastern Pacific, across the Gulf of Mexico well into the Atlantic; and by less precipitation over the western Pacific, the central Pacific away from the Tropics, Amazonia, and South Africa. During MAM, in addition to the variation associated with Pacific ITCZ that exhibits similar patterns as during DJF, the Atlantic ITCZ is more intense and farther north than normal during warm episodes. During JJA, there is more precipitation all the way across the Pacific and less precipitation over most of the southeast Asian monsoon area during warm epi-

sodes. The storm track over the northwestern Pacific is farther north than during cold episodes, bringing more precipitation over Japan and its adjacent oceanic areas during warm episodes. During SON, the SPCZ displaced markedly toward the northeast relative to cold episodes, and the Pacific ITCZ is again stronger during warm conditions. Although based on a relatively short dataset that includes only 3–6 events, the composite difference maps presented here provide us with a more spatially complete and systematic picture of the ENSO-related interannual variability in large-scale precipitation over the globe than has been possible in the past. Most variations shown here are in general agreement with previous studies by Ropelewski and Halpert (1987, 1989), which were based on historical station observations. However, the results shown in Fig. 17 enable us to see more of the full spatial character of the coherent ENSO-related variability over the globe, even though the short period of record makes statistical significance difficult to assess.

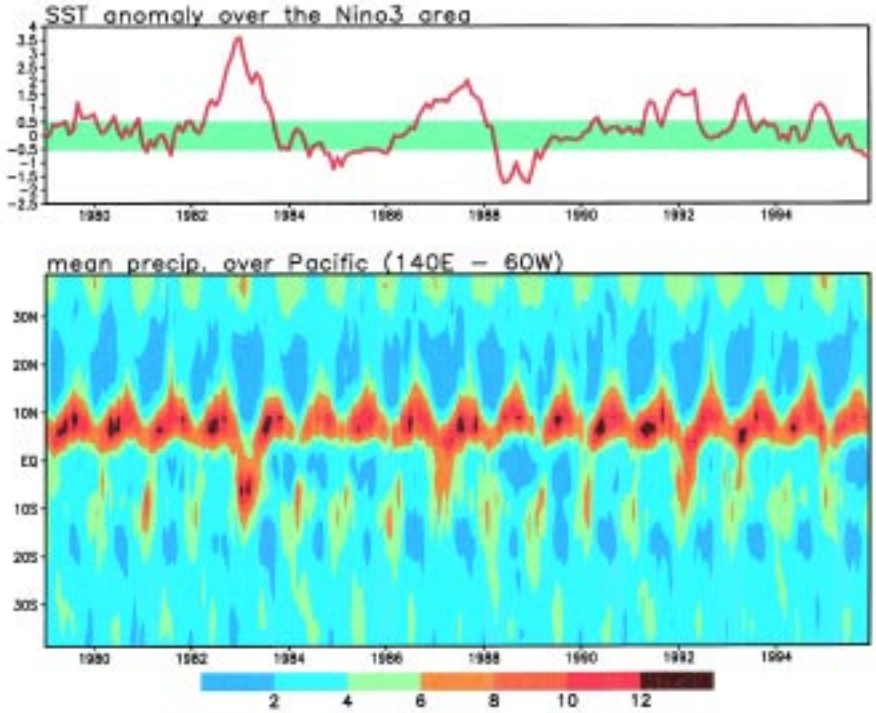

FIG. 16. Time series of the SST anomaly over the Niño 3 area (5°S–5°N; 150°–90°W) (top) and the time–latitude diagram for the precipitation (in mm day^{-1}) averaged over the Pacific section from 140° to 60°W (bottom).

5. Conclusions

Global monthly precipitation analyses have been constructed on a 2.5° lat–long grid for the 17-yr period from 1979 to 1995 by merging seven kinds of individual data sources with different characteristics. These include gauge-based monthly analyses from the Global Precipitation Climatology Centre as well as the extension discussed by Xie et al. (1996), estimates inferred from a variety of satellite observations, and the precipitation distributions from the NCEP–NCAR reanalysis. Named the CPC Merged Analysis of Precipitation (CMAP), the 17-yr dataset provides global monthly precipitation distributions with full coverage and improved quality compared to the individual data sources.

Investigation showed no apparent systematic differences in spatial distributions or discontinuities in time series in the 17-yr dataset of the CMAP despite the different data sources used for the different periods. Verification of the CMAP with a nearly independent gauge dataset confirmed its high quality over land areas. Comparisons with the merged analysis of Huffman et al. (1997) showed close agreement between the two datasets over land and over tropical and subtropical ocean areas, while significant differences were found over the extratropical oceans.

The 17-yr CMAP dataset was used to investigate the annual and interannual variability in large-scale precipitation over the globe. The distributions of seasonal and annual mean precipitation resemble those observed in the published long-term means of Jaeger (1976) and Legates and Willmott (1990) but with major differences over oceans, especially over the eastern Pacific. The annual global mean precipitation is 2.69 mm day^{-1}, with values of 1.86 (3.01) over land (oceans). The interannual variability associated with the ENSO phenomenon is similar to that found by previous studies but with much more coherent detail over the oceans.

More work is needed to improve the quality of the CMAP and to further extend its temporal coverage. Since the final quality of the merged analysis is pri-

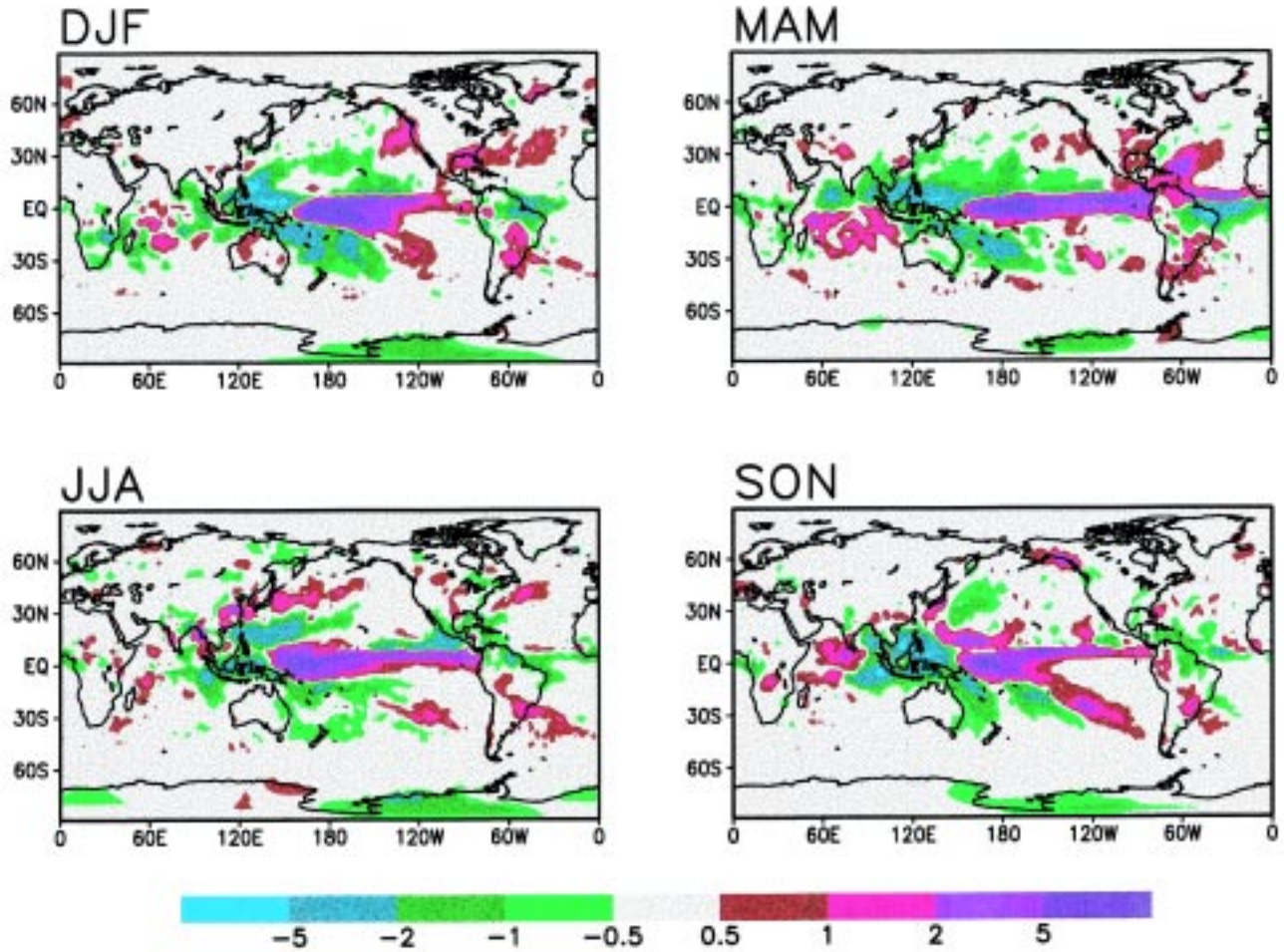

FIG. 17. Differences between warm and cold ENSO episodes during the 17-yr period from 1979 to 1995 for DJF, MAM, JJA, and SON precipitation. Areas wetter (drier) during warm ENSO episodes, with differences larger than 0.5 mm day^{-1}, are indicated by heavy (light) shading.

marily determined by the quality of the input data sources, improvements of the individual data sources are essential, especially over mid- and high latitudes where no observation-based data sources provide coverage with reasonable quality. The accurate definition of the bias and error structures for the individual data sources is the key to the success of the merged analysis. At present, this is based largely on subjective assumptions, particularly over the oceans. Further work is necessary to improve our quantitative understanding of the individual error structures. Particularly, the relationship among the error for various individual data sources must be investigated and included in the definition of the linear combination coefficients used in the maximum likelihood estimation. The observations to be made available from the TRMM project (Simpson et al. 1988) will certainly be crucial in solving this problem, at least for the Tropics and subtropics. Finally, since some applications in meteorology and hydrology require higher resolution in space and time, development of a global precipitation dataset with finer resolution is under consideration.

Acknowledgments. The authors would like to express their thanks to C. Ropelewski and J. Janowiak of the Climate Prediction Center and A. Gruber of the National Environmental Satellite, Data and Information Service of NOAA for invaluable discussions throughout this research. Comments by Dr. George Hoffman, Professor Mark Morrissey, and R. Ferraro were very helpful in improving our original manuscript. Readers interested in the dataset described in this paper may contact the first author for its availability and updated information.

References

Adler, R. F., A. J. Negri, P. R. Keehn, and I. M. Hakkarinen, 1993: Estimation of monthly rainfall over Japan and surrounding waters from a combination of low-orbit microwave and geosynchronous IR data. *J. Appl. Meteor.*, **32,** 335–356.

——, G. J. Huffman, and P. R. Keehn, 1994: Global rain estimates from microwave adjusted geosynchronous IR data. *Remote Sens. Rev.*, **11,** 125–152.

——, C. Kidd, M. Goodman, G. Petty, and M. Morrissey, 1996: PIP-3 intercomparison results. *PIP-3 Workshop*, College Park, MD, NASA, 20 pp.

Arkin, P. A., 1979: The relationship between fractional coverage of high cloud and rainfall accumulations during GATE over the B-scale array. *Mon. Wea. Rev.*, **107,** 1382–1387.

——, and B. N. Meisner, 1987: The relationship between large-scale convective rainfall and cold cloud over the western hemisphere during 1982–84. *Mon. Wea. Rev.*, **115,** 51–74.

——, and P. E. Ardanuy, 1989: Estimating climatic-scale precipitation from space: A review. *J. Climate,* **2,** 1229–1238.

——, and P. Xie, 1994: The Global Precipitation Climatology Project: First Algorithm Intercomparison Project. *Bull. Amer. Meteor. Soc.*, **75,** 401–419.

——, R. Joyce, and J. E. Janowiak, 1994: IR techniques: GOES Precipitation Index. *Remote Sens. Rev.*, **11,** 107–124.

Arpe, K., 1991: The hydrological cycle in the ECMWF short-range forecasts. *Dyn. Atmos. Oceans,* **16,** 33–60.

Barrett, E. C., and D. W. Martin, 1981: *The Use of Satellite Data in Rainfall Monitoring.* Academic Press, 340 pp.

Chang, A. T., L. S. Chiu, and G. Yang, 1995: Diurnal cycles of oceanic precipitation from SSM/I data. *Mon. Wea. Rev.*, **123,** 3371–3380.

Chiu, L. S., A. Chang, and J. E. Janowiak, 1993: Comparison of monthly rain rates derived from GPI and SSM/I using probability distribution functions. *J. Appl. Meteor.*, **32,** 323–334.

Daly, C., R. P. Neilson, and D. L. Phillips, 1994: A statistical-topographic model for mapping climatological precipitation over mountainous terrain. *J. Appl. Meteor.*, **33,** 140–158.

Dodge, J., 1994: The WetNet Project. *Remote Sens. Rev.*, **11,** 5–21.

Ferraro, R. R., N. C. Grody, and G. F. Marks, 1994: Effects of surface conditions on rain identification using SSM/I. *Remote Sens. Rev.*, **11,** 195–209.

——, and G. F. Marks, 1995: The development of SSM/I rain rate retrieval algorithms using ground-based radar measurements. *J. Atmos. Oceanic Technol.*, **12,** 755–770.

Gates, W. L., 1992: The Atmospheric-Model Intercomparison Project. *Bull. Amer. Meteor. Soc.*, **73,** 1962–1970.

Grody, N. C., 1991: Classification of snow cover and precipitation using the Special Sensor Microwave Imager. *J. Geophys. Res.*, **96,** 7423–7435.

Huffman, G. J., 1997: Simple estimates of root-mean-square random error for finite samples of estimated precipitation. *J. Appl. Meteor.*, in press.

——, G. J., R. F. Adler, B. R. Rudolf, U. Schneider, and P. R. Keehn, 1995: Global precipitation estimates based on a technique for combining satellite-based estimates, rain gauge analysis, and NWP model precipitation information. *J. Climate,* **8,** 1284–1295.

——, and Coauthors, 1996: The Global Precipitation Climatology Project (GPCP) combined precipitation dataset. *Bull. Amer. Meteor. Soc.*, **77,** 5–20.

Jaeger, L., 1976: Monatskarten des Niederschiags fur die ganze Erde. *Berichte des Deutscher Wetterdienstes,* Offenbach, 33 pp. and plates.

Janowiak, J. E., 1992: Tropical rainfall: A comparison of satellite derived rainfall estimates with model precipitation forecasts, climatologies, and observations. *Mon. Wea. Rev.*, **120,** 448–462.

——, P. A. Arkin, P. Xie, M. L. Morrissey, and D. R. Legates, 1995: An examination of the east Pacific ITCZ rainfall distribution. *J. Climate,* **8,** 2810–2823.

Joyce, R., and P. A. Arkin, 1997: Improved estimates of tropical and subtropical precipitation using the GOES Precipitation Index. *J. Atmos. Oceanic Technol.*, **14,** 997–1011.

Kalnay, E., and Coauthors, 1996: The NCEP/NCAR 40-year Reanalysis Project. *Bull. Amer. Meteor. Soc.*, **77,** 437–472.

Legates, D. R., and C. J. Willmott, 1990: Mean seasonal and spatial variability in gauge corrected global precipitation. *Int. J. Climatol.*, **10,** 111–127.

Morrissey, M. L., and X. Greene, 1991: The Pacific atoll raingage data set. Tech. Rep. Univ. Hawaii, Manoa, Honolulu, Hawaii.

Oki, R., and A. Sumi, 1994: Sampling simulation of TRMM rainfall estimation using radar-AMeDAS composites. *J. Appl. Meteor.*, **33,** 1597–1608.

Reynolds, R. W., 1988: A real-time global sea surface temperature analysis. *J. Climate,* **1,** 75–86.

Richards, F., and P. A. Arkin, 1981: On the relationship between satellite-observed cloud cover and precipitation. *Mon. Wea. Rev.*, **109,** 1081–1093.

Ropelewski, C. F., and M. S. Halpert, 1987: Global and regional scale precipitation patterns associated with El Niño/Southern Oscillation. *Mon. Wea. Rev.*, **115,** 1606–1626.

——, and ——, 1989: Precipitation patterns associated with high index phase of the Southern Oscillation. *J. Climate,* **2,** 268–284.

——, J. E. Janowiak, and M. S. Halpert, 1985: The analysis and display of real time surface climate data. *Mon. Wea. Rev.*, **113,** 1101–1106.

Rudolf, B., H. Hauschild, W. Rueth, and U. Schneider, 1994: Terrestrial precipitation analysis: Operational method and required density of point measurements. *NATO ASI Series,* **126,** 173–186.

Schubert, S., R. Rood, and J. Pfaendtner, 1993: An assimilated dataset for earth sciences applications. *Bull. Amer. Meteor. Soc.*, **74,** 2331–2342.

Sevruk, B., 1989: Reliability of precipitation measurements. Proc. *WMO/IAHS/ETH Workshop on Precipitation Measurements,* St. Moritz, Switzerland, WMO, 13–19.

Shepard, D., 1968: A two-dimensional interpolation function for irregularly spaced data. *23rd Natl. Conf. of American Computing Machinery,* Princeton, NJ.

Simpson, J., R. F. Adler, and G. R. North, 1988: A proposed tropical rainfall measuring mission. *Bull. Amer. Meteor. Soc.*, **69,** 278–295.

Spencer, R. W., 1993: Global Oceanic precipitation from the MSU during 1979-91 and comparisons to other climatologies. *J. Climate,* **6,** 1301–1326.

Vose, R. S., R. L. Schmoyer, P. M. Steurer, T. C. Peterson, R. Heim, T. R. Karl, and J. K. Eischeid, 1992: The Global Historical Climatology Network: Long-term monthly temperature, precipitation, sea-level pressure, and station pressure data. Rep. ORNL/CDIAC-53, Carbon Dioxide Inf. Anal. Cent., Oak Ridge Natl. Lab., Oak Ridge, TN, 25 pp. [Available from Carbon Dioxide Information Analysis Center, Oak Ridge National Laboratory, Oak Ridge, TN 37831-6335.]

Weng, F.-Z., R. Ferraro, and N. Grody, 1994: Global precipitation evaluation using Defense Meteorological Satellite Program F10 and F11 Special Sensor Microwave Imager (SSM/I). *J. Geophys. Res.,* **99,** 25 535–25 551.

Wilheit, T. J., A. T. C. Chang, and L. S. Chiu, 1991: Retrieval of the monthly rainfall indices from microwave radiometric measurements using probability distribution functions. *J. Atmos. Oceanic Technol.,* **8,** 118–136.

World Climate Research Programme, 1993: Global observations, analyses and simulation of precipitation. Rep. WCRP-78, WMO/TD 544, World Meteor. Org., Geneva, XX pp.

Xie, P., and P. A. Arkin, 1995: An intercomparison of gauge observations and satellite estimates of monthly precipitation. *J. Appl. Meteor.,* **34,** 1143–1160.

——, and ——, 1996: Analyses of global monthly precipitation using gauge observations, satellite estimates, and numerical model predictions. *J. Climate,* **9,** 840–858.

——, and ——, 1997: Global monthly precipitation estimates from satellite-observed Outgoing Longwave Radiation. *J. Climate,* in press.

——, B. Rudolf, U. Schneider, and P. A. Arkin, 1996: Gauge-based monthly analysis of global land precipitation from 1971–1994. *J. Geophys. Res.,* **101**(D14)**,** 19 023–19 034.